Version of Record: https://www.sciencedirect.com/science/article/pii/S001793102100836X
Manuscript_b526d26133458b52a89d366585ae6b44

Flow boiling transient critical heat flux tests with stainless steel and FeCrAl: Transient correlation implementation, model calibration, and sensitivity analysis*

Soon K. Lee,[1, 2] Nicholas R. Brown[1, 3]

[1] University of Tennessee, Knoxville, TN, USA
[2] University of New Mexico, Albuquerque, NM, USA
[3] Oak Ridge National Laboratory, Oak Ridge, TN, USA

Corresponding Author: Nicholas R. Brown, nbrown49@utk.edu

Abstract

Steady-state and transient internal-flow critical heat flux (CHF) experiments were carried out under two flow conditions, at atmospheric pressure, on 316 stainless steel (316-SS) and iron-chromium-aluminum (FeCrAl) tubes. Slow power transients at a low mass flow ($300\ kg/m^2-s$) with very low subcooling ($X_e = -0.0054$) generated premature CHFs, which were prevented by faster power transients and high mass flow ($1{,}000\ kg/m^2-s$). The measured transient CHFs increased linearly with increasing power transients, compared with the steady-state CHF. Yet, the wall superheat at the CHFs decreased with faster power transients. Transient CHF correlations highlighting heterogeneous spontaneous nucleation were calibrated to the measured CHFs and compared with other existing correlations. Transient CHF multipliers were acquired from pool and flow boiling empirical CHF correlations that were generated. The multipliers were applied to the RELAP5-3D nuclear system code to analyze the discrepancies between the measured data and the predicted CHF and post-CHF behavior, which improved peak cladding temperature predictions by 24.6%. A variance-based global sensitivity study perturbing the experimental uncertainties and cladding material thermal properties showed the diminishing influence of flow boiling heat transfer with increasing power transients, highlighting the significance of the volumetric heat capacity for the cladding integrity during transients. Transient CHF correlations were applied to the

* This manuscript has been co-authored by UT-Battelle, LLC, under contract DE-AC05-00OR22725 with the US Department of Energy (DOE). The US government retains and the publisher, by accepting the article for publication, acknowledges that the US government retains a nonexclusive, paid-up, irrevocable, worldwide license to publish or reproduce the published form of this manuscript, or allow others to do so, for US government purposes. DOE will provide public access to these results of federally sponsored research in accordance with the DOE Public Access Plan (http://energy.gov/downloads/doe-public-access-plan).

© 2021 published by Elsevier. This manuscript is made available under the Elsevier user license
https://www.elsevier.com/open-access/userlicense/1.0/

most limiting design basis accident: a hot-zero-power reactivity-initiated accident on a generic pressurized water reactor RELAP5-3D model.

Keywords: Accident-tolerant fuel; transient critical heat flux; reactivity-initiated accident

1. Introduction

The reactivity-initiated accident (RIA) is a postulated design-basis accident (DBA), typically caused by a rapid reactivity insertion due to a control rod ejection in a pressurized water reactor (PWR). A rapid control rod ejection may introduce super-prompt criticality to the reactor, causing exponential reactor power escalation in tens of milliseconds [1]. Drastic power escalation results in a near-adiabatic fuel temperature rise, introducing the possibility of a pellet cladding mechanical interaction due to the UO_2 thermal expansion [2-4]. Transient fuel-to-cladding heat transfer induces a sharp temperature gradient on the cladding-coolant interface, activating nucleation sites to initiate a transient boiling regime advancement from forced convection to departure from nucleate boiling (DNB) [5-7]. The formation of a vapor layer near the heated cladding surface as a result of DNB reduces the fuel-to-coolant heat removal rate and increases the overall fuel system temperature. The rapid rise in fuel system temperature results in fission gas release, which increases the internal pressure, and thermal-mechanical stress, which degrades the cladding integrity [1, 4, 8, 9]. While PWRs have prompt and inherent reactivity feedback mechanisms to counteract a drastic reactivity insertion, it is likely that the cladding surface will exhibit a critical heat flux (CHF), and possibly fail, during the post-CHF response to the RIA.

Recent studies have been performed to examine possible impacts on CHF caused by the use of accident-tolerant fuel (ATF) cladding [10-15]. Recent efforts [16-18] to extend the peak rod average burnup level above the current regulatory limits (62 GWd/MTU) to enhance the economic competitiveness of commercial reactors indicate that all DBAs will eventually have to be considered, including RIAs. Our work is impactful for nuclear reactor safety because it improves quantification of the margin to fuel failure for the high-temperature phase of an RIA. Best-estimate predictions of CHF phenomena require a robust transient CHF model [10], mechanistic predictions of fuel failure, and understanding of the thermal-hydraulic response to a transient power insertion. Our work uniquely demonstrates the capability of transient CHF prediction in a thermal hydraulics system code by using an empirical correlation between transient and steady-state CHFs at atmospheric pressure. In addition, we calibrate boiling models to enable more accurate predictions of cladding temperature response to the transient power insertion. The methods demonstrated in this paper can be further extended to better

predict the thermal-hydraulic behavior of cladding during the transient accident progression analysis in PWR environments.

Traditionally, hydrodynamic instability has been known to cause CHF [19]. Pool boiling transient CHF studies have revealed the limitations of CHF correlations based on fully developed nucleate boiling (FDNB), as the transient boiling characteristics induced by transient heat input were not captured [19-23]. The rapid levitation of the liquid sub-layer on a heated surface by explosive-like heterogeneous spontaneous nucleation (HSN) in cavities triggers a delay in transient CHF compared with steady-state FDNB-based CHF. Transient CHF studies account for the exponential power increase, or exponential period, of the power transient, τ. For rapid nuclear reactor transients, the exponential period can be determined from a point kinetics approximation of the prompt jump when the nuclear reactor power rises exponentially as a function of $Q \propto e^{t/\tau}$ [24, 25]. Recent studies of both pool and flow boiling transient CHF showed representative empirical correlations accounting for the exponential period and the steady-state CHF [23, 26-29]. Those studies showed good agreement between the experimental data set and the exponential period based on empirical correlations for both pool and flow boiling conditions.

Given the lack of mechanistic transient CHF models in widely used thermal-hydraulics codes (e.g., RELAP5-3D and COBRA-TF), a previous comparison study of experimental and simulated CHF experiments implemented the Groeneveld look-up table to predict low-pressure transient CHF experiments in computer models [30]. A sensitivity study over the wide range of model uncertainties revealed the conservativeness of predictions of a post-CHF temperature excursion, with large discrepancies in CHF and post-CHF behavior predictions. Such large discrepancies are inevitable, as the CHF is a function of more than pressure, mass flux, and equilibrium quality [31].

This study further investigated experimental steady-state and transient CHF and post-CHF measurements for 316 stainless steel (316-SS) tubes at two different flow conditions under increasing transient power insertions. It also conducted comparisons against an existing transient data point using an iron chromium aluminum (FeCrAl) alloy tube. Various transient power insertions were modeled in the widely used thermal-hydraulics code Reactor Excursion Leak Analysis Program (RELAP5-3D). The modeling was conducted to understand the discrepancies between the experiments and simulations, and to further reduce discrepancies by implementing transient CHF correlations based on the exponential period and on boiling heat transfer model calibrations. Using the uncertainty quantification tool Risk Analysis and Virtual Environment (RAVEN) coupled to the RELAP5-3D model of the experiment, sensitivity studies were conducted over the range of uncertainties in boiling heat transfer and thermal properties (heat capacity and thermal conductivity). The experimental uncertainties, model uncertainties, and material thermal property uncertainties were considered to understand the sensitivity of these parameters to the key figure of merit: the peak cladding temperature (PCT) under increasing transient power

insertions. Finally, transient CHF correlations were applied as a scoping study of a generic RIA in a PWR model to show the potential implications of the transient CHF multipliers for the fuel system thermal-hydraulic response.

2. Experiment and simulation descriptions

2.1. Flow boiling experiments

2.1.1. Experimental apparatus, measurement and procedure

The experiments in this paper were conducted using a flow boiling apparatus at the University of New Mexico (UNM). A detailed description of the UNM flow boiling apparatus is discussed in the literature [32, 33]. The flow loop consisted of the following components: a steam separating reservoir, a heat exchanger, a pump, a heater, an orifice flow meter, a power supply, a data acquisition system, pressure and temperature instrumentation, and a test section. The test section was made of a 508.0 mm long, 0.254 mm thick 316-SS tube with K-type thermocouples attached to measure the inlet and outlet coolant temperatures and surface temperatures. Transducers measuring the voltage and current across the heated section were implemented for data acquisition for inserted transient power through the direct-current (DC) power supply. The test section was fully insulated with thermal blocks. The deionized water coolant flowed through the tube internally with an uncertainty in velocity of ± 2 % and inlet temperature uncertainty of ± 0.2 K. The DC power was supplied through copper power terminals to the heated length of 50.8 mm. A fully developed flow was ensured by providing an inlet length of 254.0 mm prior to the heated surface. The thermocouples measuring the tube surface temperature were placed at the top end of the heated section and at the center of the heated test section for steady-state CHF experiments and for transient CHF experiments, respectively. The thermocouple locations for transient cases were designed to simplify transient CHF detection and calculation, as CHF may not occur at the end of the heated length during the transient power insertion. The acquisition rate of 80 Hz was employed to capture the transient flow boiling phenomena. All the experiments were conducted at the atmospheric pressure (84 kPa at an altitude of 1,615 m).

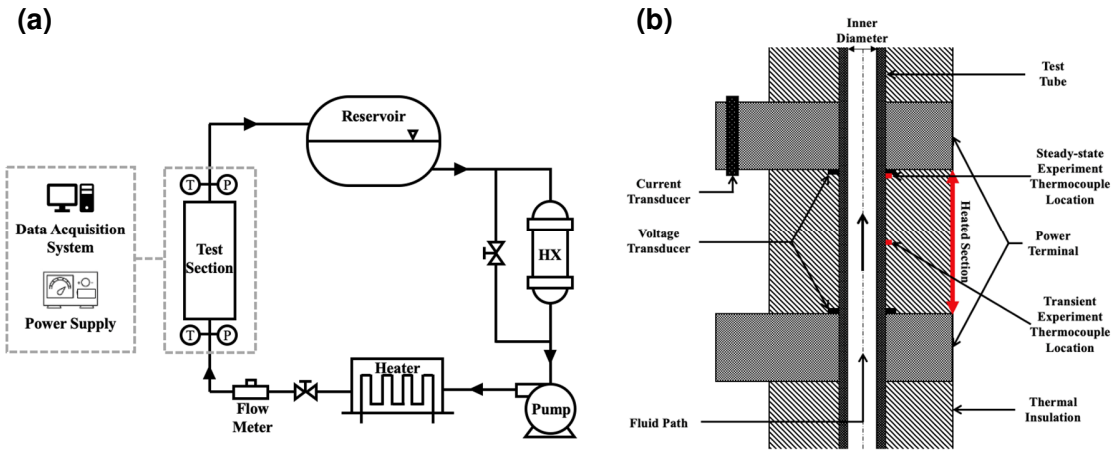

Figure 1. (a) Flow boiling loop diagram and (b) cross-sectional view of the test section [33].

Steady-state CHF experiments were conducted at a fixed inlet temperature of 40°C and at mass fluxes of 300 kg/m^2·s and 1,000 kg/m^2·s. A power increment rate of 0.01 V per 40 s was implemented until CHF was reached, which is determined by the sudden temperature jump relative to the unit time change exceeding 25 K/s (dT/dt). Power supply is shut down immediately after the CHF detection to protect the test specimen from burnout failure. The transient CHF experiments were conducted at the same mass fluxes as the steady-state experiments. The inlet quality was adjusted to match the equilibrium quality of the steady-state CHF points, assuming the thermodynamic quality at the time of DNB did not change significantly during transients [32, 34]. This setting enabled an impartial comparison between steady-state and transient CHFs under the reference conditions: pressure, flow, and quality. The transient CHF was quantified following the method presented in the previous study [32], which detects a sharp increase in the cladding temperature compared to the preceding timestep. This sharp temperature rise is presented in the Figure 5 (a) at 0.4 s and is led by the heat transfer deterioration due to boiling regime transition from nucleate to film boiling.

Table 1. Flow boiling CHF experiment conditions.

	Steady-state		Transient	
Mass flow (kg/m^2·s)	300	1,000	300	1,000
Inlet quality (–)	–0.0750		–0.0054	–0.0423
Equilibrium quality at CHF (–)	–0.0054	–0.0423		
System pressure (kPa)	84		84	

Power insertion (–)	0.01V/40s increment until CHF occurred	Haft-sine shaped power pulses (1 s width)

The steady-state heat flux was quantified using the following expression:

$$q'' = \frac{\Delta V I}{\pi D L}, \quad (1)$$

where $\Delta V, I, D,$ and L are the voltage of the heated section, DC in the circuit, inner diameter of the tube, and length of the heated section, respectively. Equilibrium quality (X_e) at the CHF location (z_{CHF}) was quantified using

$$X_e(z_{CHF}) = \frac{h_m^+(z_{CHF}) - h_f}{h_{fg}}, \quad (2)$$

where $h_f, h_{fg},$ and h_m^+ are, respectively, the saturated liquid enthalpy, the enthalpy of vaporization, and the mixture enthalpy, which is obtained from the energy balance:

$$h_m^+(z_{CHF}) = h_{in} + \frac{1}{\dot{m}} \int_0^{z_{CHF}} q' dz, \quad (3)$$

where $h_{in}, \dot{m},$ and q' are the inlet enthalpy, the mass flow rate, and the linear heat rate in the test section, respectively. Power insertion was closed when the temperature overshoot was observed from the thermocouple attached on the heated section.

The transient heat flux was quantified using the transient energy balance:

$$q''_{tr} = \frac{\Delta V I - M c_p \frac{dT}{dt}}{\pi D L}, \quad (4)$$

where $M, c_p, T,$ and t are the heated section mass, the specific heat of 316-SS, the measured temperature, and the measured time, respectively. Tube inner surface temperature was computed using the following transient conduction equation with the implicit finite difference method (FDM), implementing the Neumann boundary condition using the measured outer surface temperature and the calculated transient heat flux:

$$\frac{1}{r}\frac{d}{dr}\left(kr\frac{\partial T}{\partial r}\right) + \dot{q} = \rho c_p \frac{\partial T}{\partial t}, \quad (5)$$

where $r, k,$ and ρ are the radius, the thermal conductivity, and the density of 316-SS, respectively. One hundred discretized nodes in the tube domain were used to derive the FDM with converged results. The transient CHF is determined

2.1.2. Transient power pulses

The transient power levels of half-sine-shaped power curves with 1 s pulse width were considered. The transient power was varied from the minimal power required to observe CHF to the maximal power available from the power supply at a given mass flow, as shown in Table 2 and Figure 2. Transitions from the nucleate boiling regime to the film boiling regime were not detected below the minimal transient powers (Transients 1 and 6) for the considered flow conditions. Transients 1–5 and 6–9 match the flow conditions at steady-state CHFs of 300 and 1,000 kg/m^2·s, respectively. Note that the power shape was selected because it is similar to a subprompt (<1$ reactivity) hot-full-power RIA in a light water reactor (LWR). However, the employed pulse was slower than the superprompt (>1$ reactivity) or a hot-zero-power (HZP) RIA [35].

Table 2. Pulse identifiers with corresponding flow conditions and power peaks.

Transients	Mass flow (kg/m^2·s)	Equilibrium quality	Power pulse peak (10^9 W/m^3)
Transient 1–5	300	–0.0054	9.6, 12.7, 16.2, 18.1, 19.7
Transient 6–9	1,000	–0.0423	14.9, 18.7, 20.5, 22.3

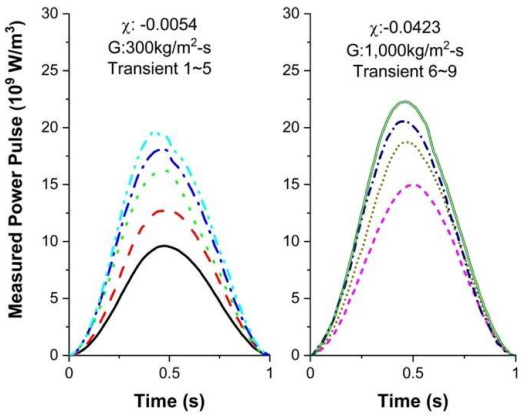

Figure 2. Power transients implemented for CHF experiments with two flow conditions.

2.2 RELAP5-3D model and sensitivity study

The experimental transient CHFs with various power pulses and flow conditions were analyzed using the best-estimate nuclear engineering system modeling tool RELAP5-3D. An effort was made to understand the discrepancies between the experimental data and the predicted CHF and post-CHF behavior by conducting a sensitivity study of heat transfer coefficients, CHF multipliers, and uncertainties

in the material thermal properties. The sensitivity was expected to highlight the implications of the considered parameters with respect to the increasing power insertions.

The RELAP5-3D model, as shown in Figure 3, consists of a time-dependent inlet volume, junctions, a vertical pipe, and a heat sink; it models the test section described in Section 2.1. A heat structure was implemented on the pipe supplying the power transients. Note that the heated lengths of the test section were simulated, as the heat transfer package of RELAP5-3D assumes fully developed steady flow. The heated length of the model was thermally insulated on the outer surface. A pipe and a heat structure using 50 axial nodes and a minimum timestep of 1E-8 s were used for model stability [30]. The maximum timestep was determined based on the Courant limit. The reference flow conditions (Table 1) were implemented. The transient power insertions in the model were implemented using the power table (in watts) constructed from the experimental power measurements. The reflood model was enabled to observe the rewetting behavior.

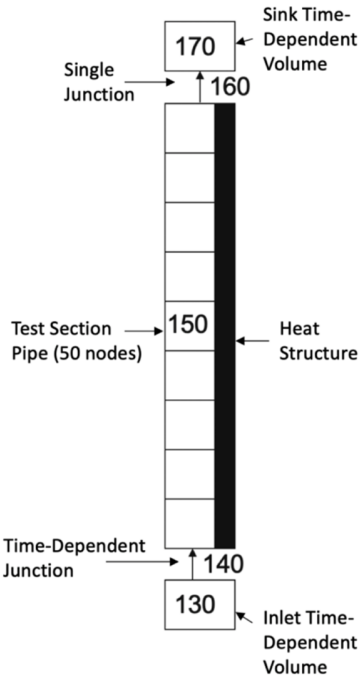

Figure 3. Nodalization diagram of RELAP5-3D model [30].

RAVEN was used to conduct the sensitivity study of the key figure of merit: PCT. Varying experimental and boiling heat transfer model uncertainties and material thermal property uncertainties may possibly impact the figures of merit. The variance-based sensitivity analysis (often referred to as the Sobol method) enabled the quantification of parametric influences as measures of sensitivity [36].

3. Experiment results and discussion

3.1 Flow boiling CHF

The steady-state boiling curves up to the CHFs were obtained by plotting the heat flux relative to the wall superheat ($T_{wall} - T_{saturation}$) at mass flows of 300 kg/m^2·s and 1,000 kg/m^2·s as shown in Figure 4. The transient CHFs at the identical flow conditions (mass flow and thermodynamic quality) are also shown in the figure. In Figure 4(a), three power pulses (transients 1–3) induced the premature CHFs, when the CHFs are lower than the steady-state CHF. Under a steady-state flow boiling condition, premature CHF occurred as a result of the boiling instabilities introduced by flow fluctuation and restriction, low-frequency oscillation, low inlet subcooling, unstable pressure fluctuation, and narrow flow channel [37-39]. As the steady-state flow condition stably induced CHFs in the repeated experiments, it was inferred that insufficient transient power insertion initiated the transition from the nucleate boiling regime to the stable film boiling regime. In the nucleate boiling initiated in a quasi-steady-state manner, effective bubble growth and detachment prompted by the forced turbulent convective forces stabilized the boiling process and prevented the coalescence of bubbles into the vapor film. In contrast, a sudden initiation of nucleation caused by pulsed power input incurred a sharp temperature gradient in the solid–liquid interface, activating bubble growth in an enlarged number of nucleation sites without fully developed convective forces [37]. With the tested transient power pulses, the rapid vapor formation rate resulted in bubble coalescence, formulating a stable transition to the film boiling regime. However, it is clear that insufficient power transients could initiate a premature transition to the film boiling regime. No premature CHFs were observed from the 1,000 kg/m^2·s mass flow condition under the given power pulses. It was concluded that the increased wall superheating resulting from the transient CHFs was induced by HSN.

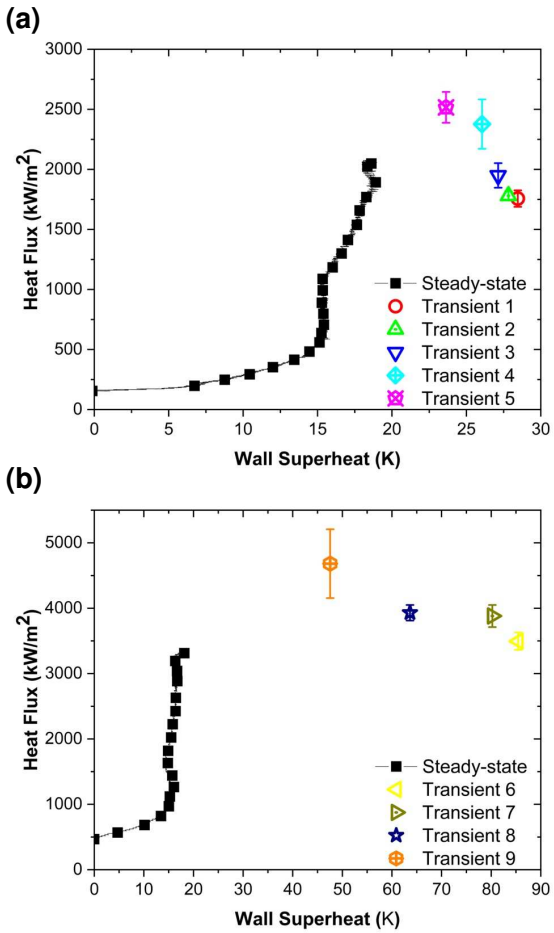

Figure 4. Steady-state boiling curves and transient CHFs at mass flows: (a) 300 kg/m^2·s and (b) 1,000 kg/m^2·s $(P = 84\ kPa)$.

Figure 5 shows the typical cladding heat transfer process and the experimental boiling curve due to a pulsed power input. During the initial power insertion, cladding temperature rapidly rises through HSN, which causes a boiling crisis and a transition to the film boiling regime with a concomitant wall superheat increase up to ~1,000 K. With a sufficient supply of coolant, the film boiling regime is sustained until the liquid quenching begins near 650 K, rapidly cooling the heated cladding surface while prompting heat transfer to the coolant. Two peaks on the heat flux curve represent the heat flux rise due to the DNB and the collapse of film boiling and complete surface rewetting.

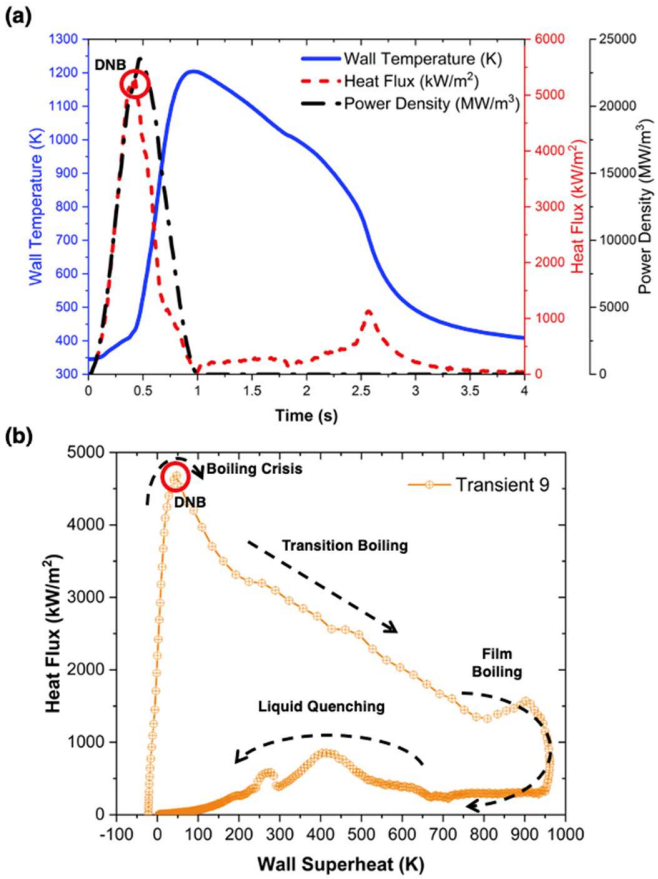

Figure 5. Transient 9: (a) Typical transient boiling heat transfer process behavior (b) boiling curve.

The experimental data showed a linear proportionality of the PCT to the measured CHFs. Durations of the film boiling regime were dependent on the CHFs and PCTs: a higher PCT induced a longer duration until the rewetting point. Following the procedure introduced in a previous study [32], prototypical transient boiling curves were constructed using the experimental measurements: CHF, rewetting point, maximum attainable heat flux during liquid quenching, and onset of single phase convection, as shown in Figure 6. In a later section, these measured points are compared with the best-estimate cases from the RELAP5-3D simulations. For both flow conditions, neither rewetting heat fluxes nor maximum attainable heat fluxes with liquid quenching showed significant variation with respect to the CHF and the power pulse. Rewetting heat flux and temperature showed only a 25% and 15% relative standard deviation (RSD) for low-mass-flow cases and 30% and 26% RSDs for high-mass-flow cases. The RSD for maximum attainable heat flux due to liquid quenching was only 15% for both heat flux and temperature in low-mass-flow conditions. Yet, the rewetting temperature increased with a rising PCT for the pulses considered [40]. A similar trend was also observed in a high-mass-flow condition, with the

exception of transient 8. It was also observed that the rise in PCT did not affect the maximum surface heat flux at a given measurement point. However, the maximum surface heat flux may vary depending on the downstream spatial location [41]. In a comparison of two flow conditions, the wall superheat at the onset of film boiling collapse increased as a result of the mass flow and inlet subcooling. The results also showed the rewetting shifted to a higher temperature and heat flux with an increase in mass flow and coolant subcooling [42].

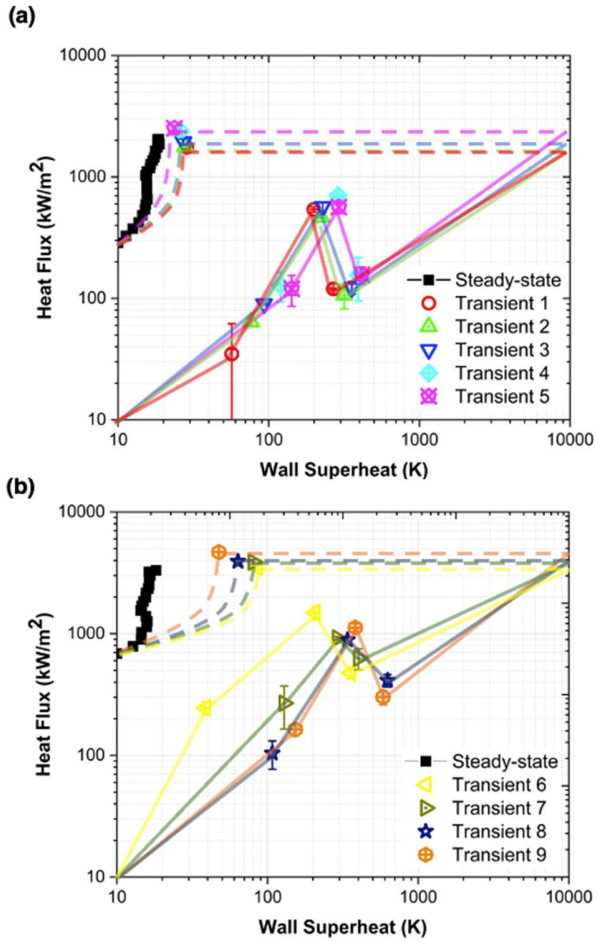

Figure 6. Steady-state boiling curves and prototypical transient boiling curves at mass flows: (a) 300 kg/m^2·s and (b) 1,000 kg/m^2·s ($P = 84\ kPa$).

3.2 Transient CHF prediction

Transient accident scenarios like RIAs trigger the reactor power to increase exponentially as a function of $Q \propto e^{t/\tau}$, where τ is the exponential period and depends on the reactivity insertion. Recent transient CHF studies revealed the dependency of τ on the exponential period in both pool and flow boiling experiments. Previous transient boiling studies showed higher CHFs resulting from faster transient power insertions [21-23, 26-29]. Transient boiling studies adopted the exponential function with the exponential period τ to simulate power insertion under RIAs, which showed an increasing $q''_{transient}/q''_{steady-state}$ ratio with decreasing τ. Sakurai explained three distinctive mechanisms for transient CHF with exponential periods [23]. For very short exponential periods, the direct transition from single-phase conduction to film boiling is prompted by HSN, and the boiling initiation heat flux equals the CHF. For longer exponential periods, the CHF is an extension of the FDNB regime on the boiling curve, and the CHF increases with a decrease in the exponential period induced by the time lag of the hydrodynamic instability. For the exponential periods between the aforementioned mechanisms, the CHF occurs as a result of the instantaneous levitation of coolant near the heated surface by HSN, before it occurs in the FDNB regime. Such empirical correlations were built based on experimental data for saturated CHFs (Eq. [6]: $P = 101 - 2063\ kPa$) and subcooled CHFs (Eq. [7]: $P = 1082\ kPa, \Delta T_{sub} = 0 - 80$), which are in the exponential period and subcooling ranges of this study:

$$q''_{tr} = q''_{st}(1 + 0.21\tau^{-0.5}). \quad (6)$$

$$q''_{tr} = q''_{st}(1 + 0.023\tau^{-0.7}). \quad (7)$$

Although the current study adopted different heating rates, the exponential periods were quantified by fitting the power density curve up to the peak in the exponential function. Estimated exponential periods from the experimental data lie in the range of HSN-induced CHFs. Figure 7 shows the experimental data compared with the empirical pool boiling CHF correlations provided by Sakurai. Note that the transient CHF value from the previous study is considered as shown (300 kg/m^2·s mass flow, –0.0068 equilibrium quality, 14.5×10^9 W/m^3 power pulse peak, 0.085 s exponential period) to show the potential material implications under the transient. The FeCrAl transient CHF cases have very similar flow conditions to those of the low mass-flow-cases. Transient 1~3 CHF data are not used for the following analysis, as the q''_{tr}/q''_{st} ratio is less than one. The experimental CHFs show relatively good agreement with the empirical correlation provided by the subcooled CHFs, as the measured CHFs are in subcooled conditions. Figure 7 also contains the best-fitted empirical correlation from the experimental data from this study:

$$q''_{tr} = q''_{st}(1 + 0.055\tau^{-0.573}). \quad (8)$$

The best-fitted correlation (Eq. 8) shows similar q''_{tr}/q''_{st} behavior under the tested exponential periods, indicating the limited implications of system pressure under the transient. It is notable that the FeCrAl transient CHF data show good agreement with both empirical correlations. Overall results highlight the significance of exponential periods and of accurate steady-state CHF predictions for predicting transient CHF. They also imply the flow transient CHFs can be predicted with HSN models under the tested flow conditions.

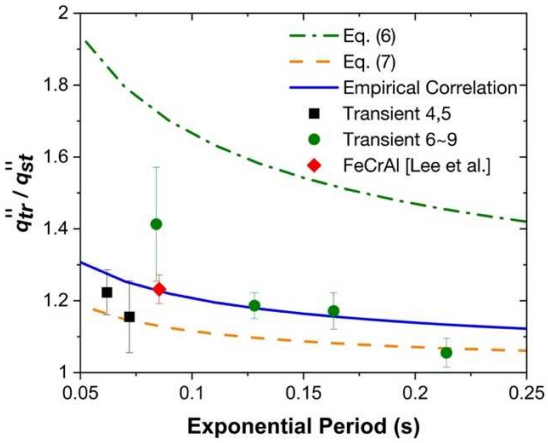

Figure 7. The relation between q''_{tr}/q''_{st} and exponential period for 316-SS at two distinct flow conditions and for a FeCrAl alloy at atmospheric pressure with pool boiling empirical correlations and a best-fitted empirical correlation.

Recent studies from Hata et al. suggested an empirical transient CHF correlation based on the steady-state CHF correlation using the exponential period under flow boiling conditions [26-28]. A transient multiplier based on the exponential period was applied to the steady-state CHF value to quantify the transient CHF, which showed good agreement over a wide range of tube geometries, heated lengths, pressures, and inlet subcoolings ($P_{in} = 718 - 1314\ kPa, \Delta T_{sub} = 68 - 161\ K, u = 4 - 13\ m/s, L/d = 5.48 - 11.08$). An identical approach was applied to the steady-state and transient CHF data in this study. First, the steady-state correlation (Eq. [9]) was verified with steady-state CHF data at two flow conditions and at atmospheric pressure [28]. The predicted steady-state CHFs showed 4.6% and 6.7% variations from the measured CHFs for 300 kg/m^2-s and 1,000 kg/m^2-s.

$$\mathrm{Bo} = \frac{q''_{st,sub}}{Gh_{fg}} = C_1 \left\{ \frac{d}{\sqrt{\sigma/g(\rho_l - \rho_g)}} \right\}^{-0.1} We^{-0.3} \left(\frac{L}{d}\right)^{-0.1} e^{-(\frac{L}{d})/(C_2 Re^{0.4})} Sc^{C_3}, \quad (9)$$

where $Bo, \sigma, We, Re, and\ Sc$ are boiling number, surface tension, Weber number, Reynolds number, and nondimensional inlet subcooling, respectively. The $C_1, C_2, and\ C_3$ constants are 0.082, 0.53, and 0.7.

Hata et al. constructed an empirical transient CHF correlation with a nondimensional CHF multiplier based on the exponential period and dimensionless characteristic length associated with Taylor instability, as shown in Eq. (10) [28]. The experimental data in their study were collected in different flow conditions. Hence, new constants corresponding to the experimental CHF data were acquired for the system code implementation.

$$\mathrm{Bo} = \frac{q''_{tr}}{Gh_{fg}} = C_1 \left\{\frac{d}{\sqrt{\sigma/g(\rho_l-\rho_g)}}\right\}^{-0.1} We^{-0.3} \left(\frac{L}{d}\right)^{-0.1} e^{-(\frac{L}{d})/(C_2 Re^{0.4})} Sc^{C_3} \times \left[1 + A\left\{\frac{\tau u}{\sqrt{\sigma/g(\rho_l-\rho_g)}}\right\}^{B}\right]. \quad (10)$$

Table 3. Constants for nondimensional transient CHF multiplier

	Constant A	Constant B
Transient 4, 5	3.729	–1.393
Transient 4, 5, and FeCrAl	0.473	–0.379
Transient 6 ~ 9	113.996	–1.555
Hata et al. [28]	11.4	–0.6

Transient CHF data points at each flow condition with a steady-state CHF were power fitted against the nondimensional exponential periods. The low-mass-flow cases showed reduced susceptibility of the exponential periods to transient CHFs compared with the high-mass-flow cases, as shown in Figure 8. For low-mass-flow cases, it was expected that both mass flux and extremely low subcooling contributed to the lower CHF enhancement in the given exponential periods. Figure 8(a) shows the best-fit correlation for transients 4 and 5 and the FeCrAl case. The addition of the FeCrAl CHF case further reduced the susceptibility of the exponential period to the transient CHF. However, it highlighted the significance of accurate steady-state CHF prediction, as the predicted transient CHFs depended greatly on the steady-state CHFs. Figure 8(b) shows the enhanced susceptibility of the exponential periods to the transient CHFs under increased subcooling and at a higher mass flow rate.

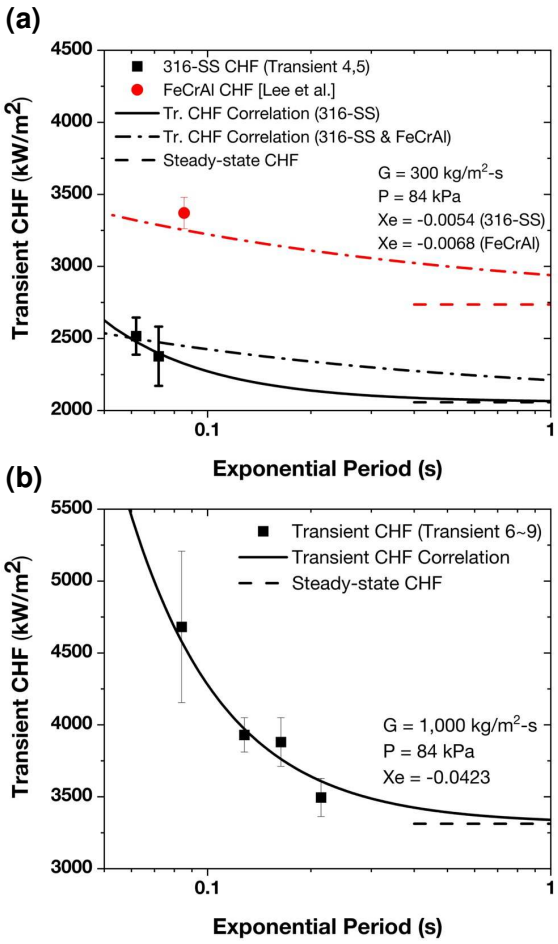

Figure 8. The relationship between transient CHFs and exponential periods at two distinct flow conditions at atmospheric pressure with flow boiling empirical correlations.

4. Simulation results and discussion

4.1 Implementation of transient CHF multiplier and model calibration

Lacking satisfactory transient CHF model implementation, current system codes predict CHF using steady-state CHF correlations, which assume CHF is caused by hydrodynamic instability. The transient CHF multiplier acquired in work described in the previous section was implemented in a RELAP5-3D simulation to account for CHF enhancement due to the exponentially increasing power. As a large reactivity insertion can induce an exponential period as small as 1 ms, introducing a method to account for the implications of transient CHF will enhance the thermal-hydraulic behavior of fuel under the transient scenarios. Figures 9 and 10 show the experimental cladding temperature response to transient power insertion with RELAP5-3D simulated results. The power pulses shown in Figure 2 are

implemented to simulate transient flow boiling. The figures contain three distinct RELAP5-3D results. The default results show the uncalibrated RELAP5-3D simulation results using the default heat transfer models given in the system code. The CHF multiplier results show the enhanced temperature prediction after the implementation of a CHF multiplier acquired from the previous flow boiling transient CHF correlations. Finally, the calibrated results show the adjustments made to the heat transfer models with the calculated CHF multiplier. Note that the thermal properties of 316-SS are linearly dependent on the temperature. In the calculations, thermal properties were extrapolated beyond the failure point to quantify the PCT prediction differences and to observe the post-CHF prediction of RELAP5-3D simulations.

Under the transient power insertion, all simulated cases overpredicted the PCT. PCT was the main figure-of-merit selected in this demonstration calibration, but it is noted that other figures of merit, like time at temperature, could also be relevant. All cases except the FeCrAl case and transient 6 exceeded the failure point of 1,673 K with given power pulses. The PCT overshoot was induced from the CHF underprediction. For high-mass-flow cases, implementation of the CHF multiplier mitigated the cladding failure by improving the temperature behavior predictions. However, the CHF multiplier implementations did not show any significant improvement in temperature predictions, as shown in Figure 9. Implementation of the CHF multiplier did not have a significant impact on either the 316-SS or the FeCrAl alloy cladding at low mass flow. For high-mass-flow cases, significantly improved PCT predictions are observed with the implementation of transient CHF multipliers, as shown in Table 4 and Figure 10. While low-mass-flow cases showed less than 2% improvements in PCT prediction, high-mass-flow cases showed an average of 24.6 % improvement by implementing the transient CHF multiplier.

Table 4. Comparison of PCTs of experimental results and RELAP5-3D predictions

	Experiment	RELAP5-3D (Default)	Difference	RELAP5-3D (CHF Multiplier)	Difference	Improvement
Transient 4	1,386 K	1,838 K	32.6 %	1,837 K	32.5%	0.1 %
Transient 5	1,494 K	1,955 K	30.8 %	1,950 K	30.5 %	0.3 %
FeCrAl	1,129 K	1,602 K	41.9 %	1,586 K	40.5 %	1.4 %
Transient 6	801 K	1,568 K	95.7 %	1,370 K	71.1 %	24.6 %
Transient 7	1,115 K	1,886 K	69.2 %	1,632 K	46.4 %	22.8 %
Transient 8	1,300 K	2,139 K	65.6 %	1,829 K	40.7 %	24.9 %
Transient 9	1,449 K	2,255 K	55.6 %	1,873 K	29.2 %	26.4 %

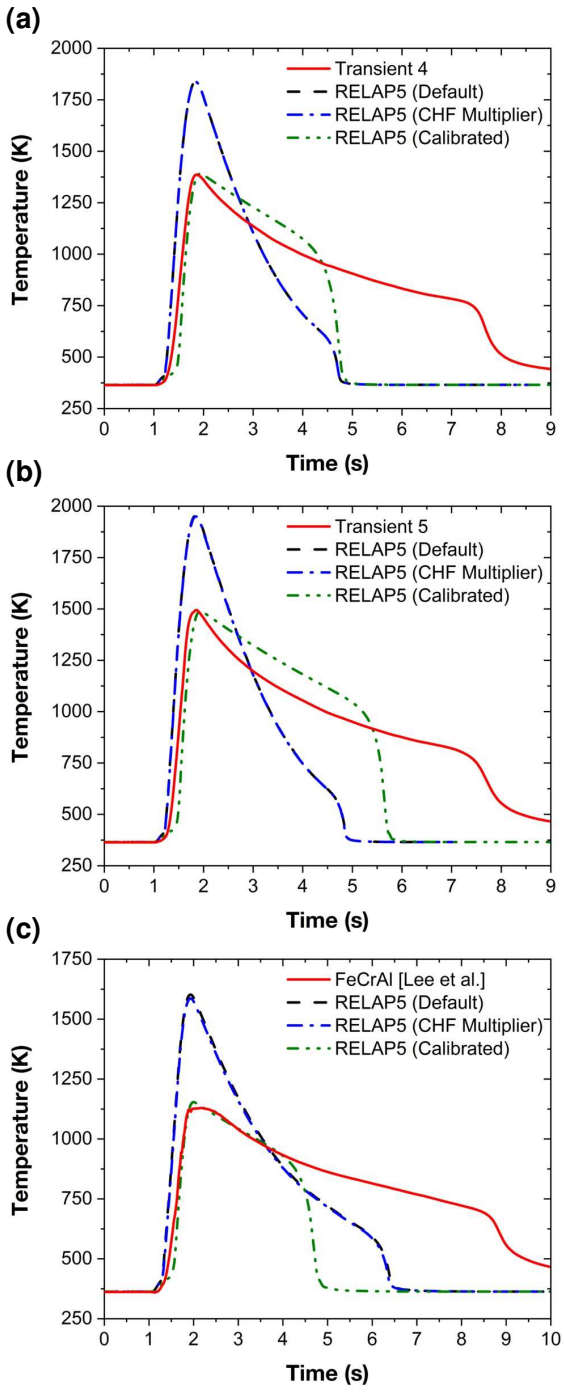

Figure 9. Experimental cladding temperature response to transient power insertion and RELAP5-3D simulated results for the (a) transient 4, (b) transient 5, and (c) FeCrAl cases ($P = 84\ kPa, X_e = -0.0423\ (316-SS), -0.0068\ (FeCrAl), G = 300\ kg/m^2 - s$).

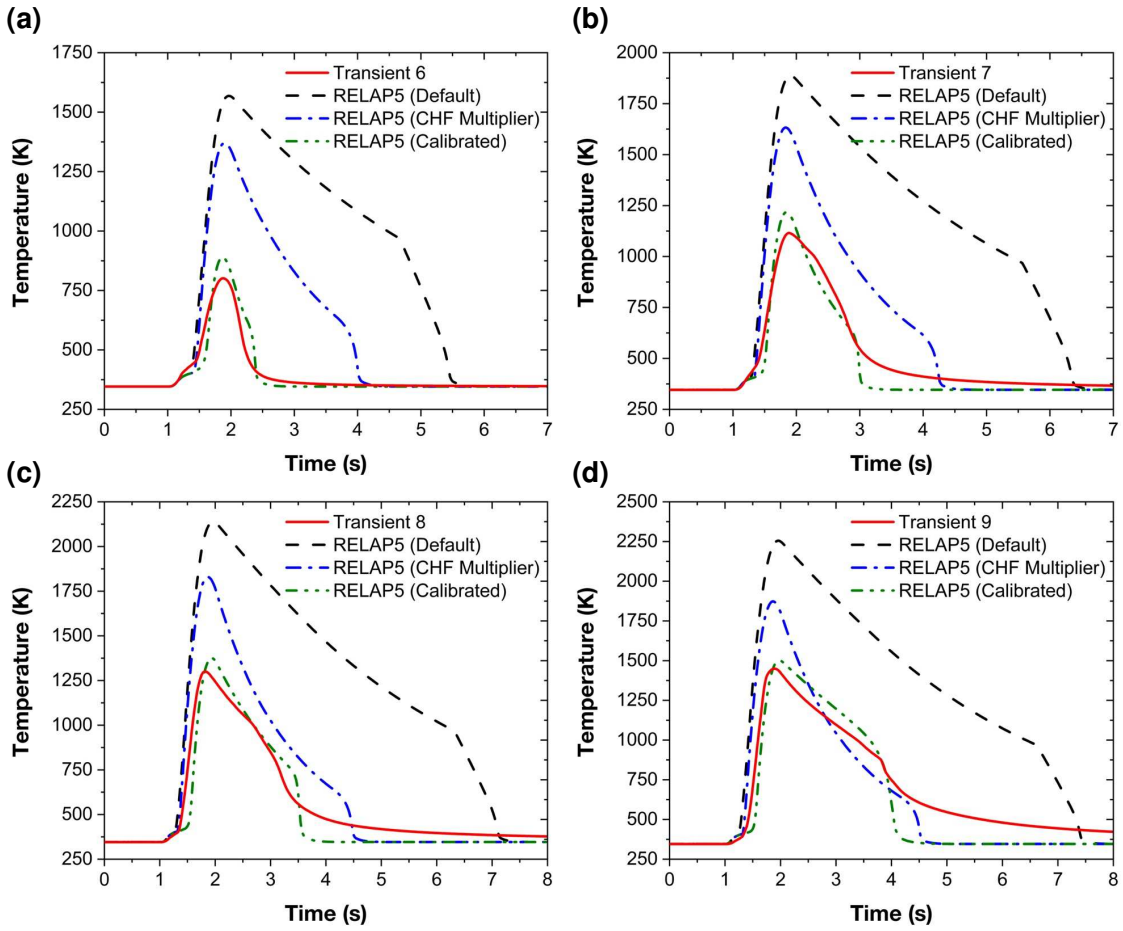

Figure 10. Experimental cladding temperature response to transient power insertion and RELAP5-3D simulated results for the (a) transient 4, (b) transient 5, and (c) FeCrAl cases ($P = 84\ kPa, X_e = -0.0423, G = 1{,}000\ kg/m^2 - s$).

Note that the low-mass-flow simulations have a rewetting point at ~1,000 K and high-mass-flow simulations have a rewetting point at ~700 K, both of which were derived from the RELAP5-3D reflood model using the modified Weisman correlation. Low mass flow resulted in an increased transition heat transfer coefficient acquired from the correlation, which overpredicted the rewetting temperature compared with the experiments. For high-mass-flow cases, the model predicted the transition boiling heat transfer coefficient and rewetting point well, with an adjusted film boiling heat transfer coefficient.

It is certain that the implementation of a CHF multiplier improved temperature prediction while maintaining a conservative PCT. The model uncertainties from the transition boiling regime and the film boiling regime contributed to insufficient temperature predictions and inaccurate predictions of the post-CHF responses compared with the experimental results. Transition boiling and film boiling multipliers

were calibrated to best match the experimental results, as shown in Table 5. In low-mass-flow cases, large transition boiling multipliers were used to reduce the overall temperature of the heated surface. Yet, the film boiling heat transfer coefficients were reduced to match the temperature behavior from the PCT to the collapse of film boiling. An enhanced transition boiling heat transfer coefficient led to a rapid temperature drop from the rewetting compared with the experimental results. In high-mass-flow cases, transition boiling heat transfer coefficients were enhanced with respect to inserted transient pulses to best match the PCT. For transient 6, the film boiling regime was not sustained because of the rapid heat transfer from the coolant with a relatively low power pulse. To match the post-CHF behavior, the film boiling heat transfer coefficient was enhanced to a high value compared with the other cases. With increasing power, film boiling heat transfer coefficients were reduced to near 0.3, following the same trend as seen in the low-mass-flow cases.

Table 5. Heat transfer coefficient multipliers for the best match cladding temperature behavior.

	Multiplier			PCT difference
	Transition boiling	CHF	Film boiling	
Transient 4	4.2	1.167	0.2	0.3 %
Transient 5	3.8	1.208	0.2	0.4 %
FeCrAl	3.9	1.188	0.3	2.2 %
Transient 6	2.0	1.084	2.8	10.9 %
Transient 7	2.5	1.130	1.5	9.2 %
Transient 8	2.9	1.203	0.8	5.7 %
Transient 9	2.9	1.412	0.35	3.6 %

4.2 Sensitivity study of transient flow boiling

To quantify the effects of boiling parameters and material properties during the transient power insertion, the cladding temperature was identified as the key figure of merit for the sensitivity analysis. The cladding temperature is the key parameter determining the material integrity in the boiling environment. The input parameters considered were forced convection heat transfer coefficient, nucleate boiling heat transfer coefficient, CHF, transition boiling heat transfer coefficient, film boiling heat transfer coefficient, and material thermal conductivity and heat capacity. The range of parametric perturbation was determined from the experimental uncertainties and the RELAP5-3D model uncertainties. From the experimental loop, forced convection had $\pm 2\%$ uncertainty. Experimental uncertainties in nucleate boiling, CHF, and film boiling were $\pm 10\%$, $\pm 12\%$, and $\pm 20\%$, respectively. Based on three repeated experiments for each transient, the most conservative uncertainty ranges were selected for each parameter. The Chen transition boiling model includes a $\pm 16\%$ deviation from the experimental data used to develop the model [44]. Finally, the 316-SS and FeCrAl alloy had measurement uncertainties of $\pm 5\%$ and $\pm 7\%$ for thermal conductivity and heat capacity, respectively [45, 46]. Manufacturing uncertainties for claddings were not considered in this study.

The results of the Sobol sensitivity analysis of the effects of transient flow boiling heat transfer regimes and material properties are shown in Figure 11. The data are the results of 249 RELAP5-3D/RAVEN sample runs. At a low-mass-flow condition, the volumetric heat capacity of the material is the key parameter dictating the evolution of the temperature overshoot during the transient. For a high-mass-flow condition, the implications of increasing power input can be observed. The key parameter impacting the PCT is again the volumetric heat capacity. However, the small impact of flow boiling heat transfers can be observed owing to the enhanced heat transfer from the coolant with low power transients. The influence of forced convection heat transfer and nucleate boiling heat transfer decreased with increasing power input, implying a diminishing influence of flow with increasing power transient and highlighting the importance of material volumetric heat capacity.

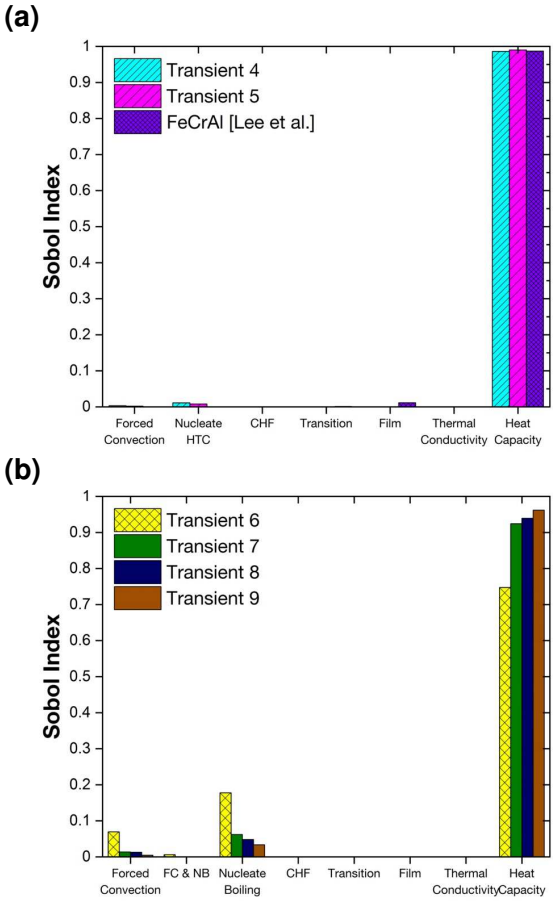

,

Figure 11. Variance-based global sensitivity results (a) 300 $kg/m^2 - s$ cases and (b) 1,000 $kg/m^2 - s$ cases.

4.3 Impact of transient CHF multiplier on RIA

An RIA that occurs under HZP conditions is expected to be limiting. With an extremely short power pulse, the coolant near the fuel system experiences a rapid transition from forced convection to the film boiling regime via a transient CHF. The transient CHF multiplier was implemented in the RELAP5-3D RIA simulation. Figure 12 shows the relative power pulses during the HZP under an RIA transient for UO_2-Zircaloy 4 and UO_2-FeCrAl fuel systems, which were calculated from the 3D core kinetics [35]. These power pulses were applied to the RELAP5-3D generic PWR models to observe the impacts of the transient CHF multiplier on the DBA [10].

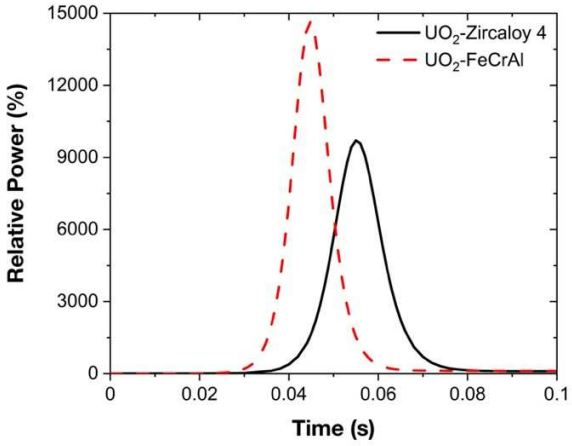

Figure 12. Relative power as a function of time for RIA.

The exponential periods were evaluated based on the full-width at half-maximum of the pulses by fitting the half-width pulse curves into an exponential curve. The evaluated exponential periods, 5.87 ms and 4.59 ms for UO_2-Zircaloy 4 and UO_2-FeCrAl, respectively, were used to quantify the CHF multipliers in both pool and flow boiling transient CHF correlations (Eq. [7] and Eq. [10]). Note that the thermal-hydraulic conditions at which these empirical correlations were constructed were different from the typical PWR HZP condition. For example, the flow boiling correlations were developed under lower pressure compared with normal PWR operating conditions, but were applied here in a scoping study to show the potential magnitude of accounting for transient CHF. Except for the pressure, the RELAP5-3D generic PWR model had inlet subcooling and flow velocity ($\Delta T_{sub} = 62\ K, u = 4.83\ m/s$) similar to the conditions under which the correlation was acquired. The transient CHF multipliers calculated from the exponential periods are shown in Table 6. Thermal-hydraulic parameters in the flow boiling correlation were acquired based on the steady-state PWR HZP condition prior to the transient. Under the same exponential period, the flow boiling correlation had higher transient CHF multiplier values than the pool boiling correlation, as it accounted for the flow velocity and had large constant values for the nondimensional transient CHF multipliers based on the experimental data.

Table 6. Exponential periods and transient CHF multipliers for RIA.

	UO_2-Zircaloy 4 fuel system	UO_2-FeCrAl fuel system
Exponential period, τ (ms)	5.87	4.59
Pool boiling CHF multiplier (Eq.[7])	1.84	2.00
Flow boiling CHF multiplier	2.29	2.66

(Eq.[10])		

An in-depth RELAP5-3D model description for the generic PWR HZP RIA simulation from the literature [10] was used for this study. The reactor consisted of a pressure vessel, two primary loops with once-through steam generators, pumps, pressurizers, and valves. The core was modeled by five channels connected by the crossflow junctions and a bypass channel. The fuel conditions in the core were at beginning-of-cycle with 2,700 MW_{th} output, 15.51 MPa system pressure, 553 K inlet coolant temperature. Ten equal-height axial nodes were used to represent the 3.568 m fuel height. In this demonstration, the Groeneveld look-up table was used for the CHF prediction method in the RELAP5-3D model to consistently implement the transient CHF multiplier.

Figure 13 shows the RELAP5-3D simulation results for the maximum fuel centerline temperature behavior and the maximum cladding surface temperature responses during the HZP RIA scenario. With increased CHF, simulations with pool and flow boiling transient CHF multipliers show reduced maximum fuel and cladding temperatures relative to the base models for both claddings. For the UO_2-Zircaloy 4 fuel system, the maximum fuel centerline temperatures show limited sensitivity to the CHF multipliers, as the fuel temperature rise was mainly driven by the transient power pulse and insufficient heat transfer to the coolant due to the CHF and post-CHF behavior. The fuel temperature responses for the UO_2-FeCrAl fuel system show enhanced significance compared with the UO_2-Zircaloy 4 fuel system, as higher thermal-conductivity and the reduced thickness of the FeCrAl cladding improved the fuel-to-coolant heat transfer.

All simulation results showed the PCT locations at subcooled film boiling regimes with different temperature responses to the transient pulses. The PCTs for the base models were predicted at 1,042 K and 1,318 K for the UO_2-Zircaloy 4 and UO_2-FeCrAl fuel systems. The base model Zircaloy 4 cladding showed a rapid cladding surface temperature rise driven by the power pulse, which quickly cooled down to ~700 K. The base model FeCrAl cladding preserved the high temperature from the reactivity insertion for a longer period compared with the Zircaloy 4 cladding base model. Such rapid cladding surface temperature rises driven by the power pulse inputs were not observed in the implementation of transient CHF multipliers for both claddings. Enhanced transient CHFs reduced the predicted PCTs in the models. The predicted PCTs for the Zircaloy 4 cladding were 789 K and 788 K for pool and flow boiling CHF correlations, respectively. The predicted PCTs for the FeCrAl cladding were 930 K and 924 K for pool and flow boiling CHF correlations, respectively. Implementation of transient CHF multipliers reduced the PCTs by 24% and 29% for Zircaloy 4 and FeCrAl claddings, respectively. The pool and flow boiling correlations did not show a significant difference in PCT predictions for either cladding. Still, the flow boiling correlations resulted in lower PCT predictions with higher CHF multipliers. The results

highlighted the sensitivity of the PCT to the transient CHF multiplier under the transient scenario. While the base case showed temperature responses below the critical point, the simulation results demonstrated that the fuel system may experience less strenuous thermal-hydraulic conditions during the RIA. It is essential to acquire experimental data at corresponding thermal-hydraulic conditions and representative pulse inputs to more accurately predict the temperature behavior relative to the exponential periods [47]. It is also recommended that data be acquired and a reflooding model be developed at the corresponding system pressure to accurately predict the fuel system response to the transient.

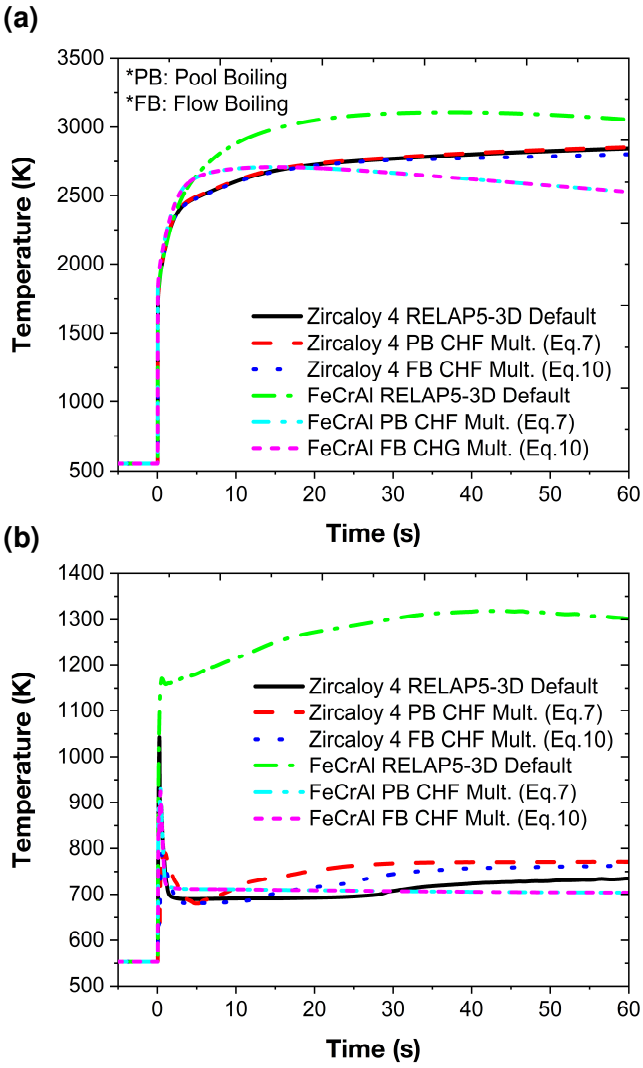

Figure 13. Impact of CHF multiplier on (a) peak fuel centerline temperature, (b) peak cladding surface temperature during simulated reactivity-initiated accident.

5. Conclusion

Steady-state internal-flow CHF experiments were conducted at two distinct flow conditions under atmospheric pressure on 316-SS cladding. Various transient power pulses with widths of 1 s were applied to the equivalent reference flow conditions, and transient CHFs were compared with steady-state CHFs. The experimental CHF results at a low-mass-flow condition with extremely low subcooling induced premature CHFs from insufficient power transients. Increasing the power pulse prevented the occurrence of premature CHFs at the given flow condition. Such events were not observed at high-mass-flow conditions, which induced increased transient CHFs compared with the steady-state CHF. The post-CHF responses showed insignificant variation relative to the measured transient CHFs and the power pulses. Rather, the onset of film boiling collapse and the rewetting behaviors were dependent on the mass flow and inlet subcooling.

The exponential heating periods were used to quantify the relationship between steady-state CHF and transient CHF. The experimentally measured CHFs were fitted to the HSN models and exponential periods. The empirical flow boiling CHFs fitted to the pool boiling correlation showed a similar trend to the existing correlation for subcooled transient CHFs, implying the possibility of predicting flow boiling transient CHFs for mass flows of up to 1,000 $kg/m^2 - s$. From the thermal-hydraulic conditions, nondimensional exponential periods were calibrated for the empirical flow boiling transient CHF correlations. Both pool and flow boiling transient CHF correlations related the exponential heating period to the ratio of transient CHF to steady-state CHF. This finding highlights that accurate prediction of steady-state CHF is crucial for detailed transient flow boiling behavior analysis, especially when the material sensitivity to CHF is significant.

The CHF multipliers were acquired from the best-fit correlations and applied to the RELAP5-3D system code simulation for the boiling model calibrations, enhancing CHF and post-CHF behavior predictions of the PCT. At low mass flow, inserted transient pulses were the dominant parameter driving the temperature rise, limiting the implication of the transient CHF multipliers. The high-mass-flow cases showed a 24.6 % improvement in PCT prediction when the transient CHF multiplier was implemented. Nonetheless, the predicted PCT was conservative compared with the experimental values. A variance-based global sensitivity analysis was carried out to measure the influence of flow boiling heat transfer parameters and cladding material thermal properties on the cladding integrity. The overall results highlighted the dominant impact of the volumetric heat capacity during the transient power insertions. Results also indicated the diminishing implication of the flow and expanding impact of the heat capacity with increasing power transients. Based on the empirical correlations, the transient CHF multipliers for a representative RIA power pulse were implemented for the generic PWR HZP RIA condition, which showed a less severe thermal-hydraulic response to the transient power pulse compared with the base model simulations for the UO_2-Zircaloy 4 and UO_2-FeCrAl fuel systems.

6. Acknowledgements

The authors acknowledge that the experimental facility at the University of New Mexico was led by Professor Youho Lee (present affiliation Seoul National University) and Professor Edward Blandford (present affiliation Kairos Power). Prof. Youho Lee of Seoul National University suggested running these experiments.

The experiments and sensitivity analysis for the study were financially supported by the Department of Energy, Nuclear Energy, University Program award 17-12688, and the data analysis and model calibration by the Department of Energy, Nuclear Energy, Advanced Fuels Campaign. The FeCrAl material was donated to the project by Oak Ridge National Laboratory [13].

All experiments were performed at the University of New Mexico and all result analysis and computer simulations were performed at the University of Tennessee. First author S. Lee performed the experiments, result analysis, and computer simulations.

Appendix A. Nomenclature

Acronyms

ATF	Accident tolerant fuel
CHF	Critical heat flux
DBA	Design-basis accident
DNB	Departure from nucleate boiling
FDM	Finite difference method
FDNB	Fully developed nucleate boiling
HSN	Heterogeneous spontaneous nucleation
HZP	Hot zero power
LWR	Light water reactor
PWR	Pressurized water reactor
PCT	Peak cladding temperature
RAVEN	Risk Analysis Virtual Environment
RELAP5-3D	Reactor Excursion Leak Analysis Program
RIA	Reactivity-initiated accident
RSD	Relative standard deviation

References

[1] OECD Nuclear Energy Agency. Organization for Economic Co-operation and Development. (2010). *Nuclear Fuel Behaviour Under Reactivity-initiated Accident (RIA) Conditions: State-of-the-art Report*. NEA/OECD.

[2] Bernaudat, C., Cambier, S., Guion, J., & Benjamin, S. (2009). An analytical criterion to prevent PCMI fuel rod cladding failure during RIA transients.

[3] Geelhood, K. J., Beyer, C. E., & Cunningham, M. E. (2004). *Modifications to FRAPTRAN to predict fuel rod failures due to PCMI during RIA-type accidents* (No. PNNL-SA-42156). Pacific Northwest National Lab.(PNNL), Richland, WA (United States).

[4] Le Saux, M., Besson, J., Carassou, S., Poussard, C., & Averty, X. (2010). Behavior and failure of uniformly hydrided Zircaloy-4 fuel claddings between 25 C and 480 C under various stress states, including RIA loading conditions. *Engineering Failure Analysis*, *17*(3), 683-700.

[5] Han, C. Y. (1962). *The mechanism of heat transfer in nucleate pool boiling* (Doctoral dissertation, Massachusetts Institute of Technology).

[6] Hsu, Y. Y. (1962). On the size range of active nucleation cavities on a heating surface. *Journal of Heat Transfer*, *84*(3), 207-213.

[7] Hernandez, R., Folsom, C. P., Woolstenhulme, N. E., Jensen, C. B., Bess, J. D., Gorton, J. P., & Brown, N. R. (2020). Review of pool boiling critical heat flux (CHF) and heater rod design for CHF experiments in TREAT. *Progress in Nuclear Energy*, *123*, 103303.

[8] Papin, J., Balourdet, M., Lemoine, F., Lamare, F., Frizonnet, J. M., & Schmitz, F. (1996). French studies on high-burnup fuel transient behavior under RIA conditions. *Nuclear Safety*, *37*(4), 289-327.

[9] Desquines, J., Koss, D. A., Motta, A. T., Cazalis, B., & Petit, M. (2011). The issue of stress state during mechanical tests to assess cladding performance during a reactivity-initiated accident (RIA). *Journal of Nuclear Materials*, *412*(2), 250-267.

[10] Liu, M., Brown, N. R., Terrani, K. A., Ali, A. F., Blandford, E. D., & Wachs, D. M. (2017). Potential impact of accident tolerant fuel cladding critical heat flux characteristics on the high temperature phase of reactivity initiated accidents. *Annals of Nuclear Energy*, *110*, 48-62.

[11] Ali, A. F., Gorton, J. P., Brown, N. R., Terrani, K. A., Jensen, C. B., Lee, Y., & Blandford, E. D. (2018). Surface wettability and pool boiling critical heat flux of accident tolerant fuel cladding-FeCrAl alloys. *Nuclear Engineering and Design*, *338*, 218-231.

[12] Seo, G. H., Jeun, G., & Kim, S. J. (2016). Enhanced pool boiling critical heat flux with a FeCrAl layer fabricated by DC sputtering. *International Journal of Heat and Mass Transfer*, *102*, 1293-1307.

[13] Lee, S. K., Liu, M., Brown, N. R., Terrani, K. A., & Lee, Y. (2020). Effect of heater material and thickness on the steady-state flow boiling critical heat flux. *Nuclear Technology*, *206*(2), 339-346.

[14] Ali, A., Kim, H. G., Hattar, K., Briggs, S., Park, D. J., Park, J. H., & Lee, Y. (2020). Ion irradiation effects on Cr-coated zircaloy-4 surface wettability and pool boiling critical heat flux. *Nuclear Engineering and Design*, *362*, 110581.
[15] Son, G. M., Kim, K. M., & Bang, I. C. (2018). Chromia coating with nanofluid deposition and sputtering for accident tolerance, CHF enhancement. *International Journal of Heat and Mass Transfer*, *118*, 890-899.
[16] Capps, N., Wysocki, A., Godfrey, A., Collins, B., Sweet, R., Brown, N., Lee, S., Szewczyk, N., & Hoxie-Key, S. (2021). Full core LOCA safety analysis for a PWR containing high burnup fuel. *Nuclear Engineering and Design*, accepted and forthcoming.
[17] Capps, N., Jensen, C., Cappia, F., Harp, J., Terrani, K., Woolstenhulme, N., & Wachs, D. M. (2020). A Critical Review of High Burnup Fuel Fragmentation, Relocation, and Dispersal under Loss-Of-Coolant Accident Conditions. *Journal of Nuclear Materials*, *546*(1).
[18] Papin, J., Balourdet, M., Lemoine, F., Lamare, F., Frizonnet, J. M., & Schmitz, F. (1996). French studies on high-burnup fuel transient behavior under RIA conditions. *Nuclear Safety*, *37*(4), 289-327.
[19] Liang, G., & Mudawar, I. (2018). Pool boiling critical heat flux (CHF)–Part 1: Review of mechanisms, models, and correlations. *International Journal of Heat and Mass Transfer*, *117*, 1352-1367.
[20] Miyasaka, Y., Inada, S., & Owase, Y. (1980). Critical heat flux and subcooled nucleate boiling in transient region between a two-dimensional water jet and a heated surface. *Journal of Chemical Engineering of Japan*, *13*(1), 29-35.
[21] Sakurai, A., & Shiotsu, M. (1977). Transient pool boiling heat transfer—Part 1: Incipient boiling superheat. *Journal of Heat Transfer*, *99*(4), 547-553.
[22] Sakurai, A., & Shiotsu, M. (1977). Transient pool boiling heat transfer—Part 2: Boiling heat transfer and burnout, *Journal of Heat Transfer*, *99*(4), 554-560.
[23] Sakurai, A. (2000). Mechanisms of transitions to film boiling at CHFs in subcooled and pressurized liquids due to steady and increasing heat inputs. *Nuclear Engineering and Design*, *197*(3), 301-356.
[24] Lamarsh, J. R. (1966). *Introduction to Nuclear Reactor Theory*. Addison-Wesley.
[25] Stacey, W. M. (2007). *Nuclear Reactor Physics* (Vol. 2). Weinheim: Wiley-VCH.
[26] Hata, K., Shiotsu, M., & Noda, N. (2006). Influence of heating rate on subcooled flow boiling critical heat flux in a short vertical tube. *JSME International Journal Series B Fluids and Thermal Engineering*, *49*(2), 309-317.
[27] Hata, K., & Masuzaki, S. (2010). Influence of heat input waveform on transient critical heat flux of subcooled water flow boiling in a short vertical tube. *Nuclear Engineering and Design*, *240*(2), 440-452.
[28] Hata, K., & Noda, N. (2008). Transient critical heat fluxes of subcooled water flow boiling in a short vertical tube caused by exponentially increasing heat inputs. *Journal of Heat Transfer*, *130*(5).

[29] Park, J., Fukuda, K., & Liu, Q. (2009). Transient CHF phenomena due to exponentially increasing heat inputs. *Nuclear Engineering and Technology*, *41*(9), 1205-1214.
[30] Gorton, J. P., Lee, S. K., Lee, Y., & Brown, N. R. (2019). Comparison of experimental and simulated critical heat flux tests with various cladding alloys: Sensitivity of iron-chromium-aluminum (FeCrAl) to heat transfer coefficients and material properties. *Nuclear Engineering and Design*, *353*, 110295.
[31] Groeneveld, D. C., Shan, J. Q., Vasić, A. Z., Leung, L. K. H., Durmayaz, A., Yang, J., ... & Tanase, A. (2007). The 2006 CHF look-up table. *Nuclear Engineering and Design*, *237*(15-17), 1909-1922.
[32] Lee, S. K., Liu, M., Brown, N. R., Terrani, K. A., Blandford, E. D., Ban, H., ... & Lee, Y. (2019). Comparison of steady and transient flow boiling critical heat flux for FeCrAl accident tolerant fuel cladding alloy, Zircaloy, and Inconel. *International Journal of Heat and Mass Transfer*, *132*, 643-654.
[33] Lee, S. K., Lee, Y., Brown, N. R., & Terrani, K. A. (2020). Elucidating the Impact of Flow on Material-Sensitive Critical Heat Flux and Boiling Heat Transfer Coefficients: An Experimental Study with Various Materials. *International Journal of Heat and Mass Transfer*, *158*, 119970.
[34] Bessiron, V. (2007). Modelling of clad-to-coolant heat transfer for RIA applications. *Journal of Nuclear Science and Technology*, *44*(2), 211-221.
[35] Brown, N. R., Wysocki, A. J., Terrani, K. A., Xu, K. G., & Wachs, D. M. (2017). The potential impact of enhanced accident tolerant cladding materials on reactivity initiated accidents in light water reactors. *Annals of Nuclear Energy*, *99*, 353-365.
[36] Sobol, I. M. (2001). Global sensitivity indices for nonlinear mathematical models and their Monte Carlo estimates. *Mathematics and Computers in Simulation*, *55*(1-3), 271-280.
[37] Sinha, D. N., Brodie, L. C., Semura, J. S., & Young, F. M. (1979). Premature transition to stable film boiling initiated by power transients in liquid nitrogen. *Cryogenics*, *19*(4), 225-230.
[38] Moon, S. K., Chun, S. Y., Park, K. Y., & Baek, W. P. (2002). Transient critical heat flux under flow coastdown in a vertical annulus with non-uniform heat flux distribution. *Nuclear Engineering and Technology*, *34*(4), 382-395.
[39] Lee, J., Jo, D., Chae, H., Chang, S. H., Jeong, Y. H., & Jeong, J. J. (2015). The characteristics of premature and stable critical heat flux for downward flow boiling at low pressure in a narrow rectangular channel. *Experimental Thermal and Fluid Science*, *69*, 86-98.
[40] Filipovic, J., Incropera, F. P., & Viskanta, R. (1995). Rewetting temperatures and velocity in a quenching experiment. *Experimental Heat Transfer An International Journal*, *8*(4), 257-270.
[41] Agrawal, C., Lyons, O. F., Kumar, R., Gupta, A., & Murray, D. B. (2013). Rewetting of a hot horizontal surface through mist jet impingement cooling. *International Journal of Heat and Mass Transfer*, *58*(1-2), 188-196.

[42] Adham-Khodaparast, K., Xu, J. J., & Kawaji, M. (1995). Flow film boiling collapse and surface rewetting in normal and reduced gravity conditions. *International Journal of Heat and Mass Transfer*, *38*(15), 2749-2760.
[43] Visentini, R., Colin, C., & Ruyer, P. (2014). Experimental investigation of heat transfer in transient boiling. *Experimental Thermal and Fluid Science*, *55*, 95-105.
[44] Idaho National Laboratory, "RELAP5-3D Code Manuals, Volumes I, II, III, IV, V, and Appendix A, Revision 4.3," Idaho National Laboratory, Idaho Falls, ID, INEEL-EXT 98-00834, 2015.
[45] Kim, C. S. (1975). *Thermophysical properties of stainless steels* (No. ANL-75-55). Argonne National Laboratory, IL. (USA).
[46] Mills, K. C., Su, Y., Li, Z., & Brooks, R. F. (2004). Equations for the calculation of the thermo-physical properties of stainless steel. *ISIJ International*, *44*(10), 1661-1668.
[47] Marcum, W., LaBrier, D., Brown, E., Yan, Y. and Woolstenhulme, N., 2020. Developing Separate Effects Transient Test Experiments Using an Out-of-Pile Flowing Water Loop. *Nuclear Technology*, *206*(6), pp.895-910.